



Food Web Functions and Interactions During Spring and Summer in the Arctic Water Inflow Region: Investigated Through Inverse Modeling

OPEN ACCESS

Edited by:

Peng Xiu,
South China Sea Institute
of Oceanology (CAS), China

Reviewed by:

Tsuyoshi Wakamatsu,
Nansen Environmental and Remote
Sensing Center, Norway
Yngvar Olsen,
Norwegian University of Science
and Technology, Norway

*Correspondence:

Kalle Olli
kalle.oli@emu.ee;
kalle.oli@ut.ee

†Present address:

Gayantonia Franzè,
Institute of Marine Research,
Flødevigen, Norway

Specialty section:

This article was submitted to
Global Change and the Future Ocean,
a section of the journal
Frontiers in Marine Science

Received: 30 November 2018

Accepted: 24 April 2019

Published: 28 May 2019

Citation:

Olli K, Halvorsen E, Vernet M,
Lavrentyev PJ, Franzè G,
Sanz-Martin M, Paulsen ML and
Reigstad M (2019) Food Web
Functions and Interactions During
Spring and Summer in the Arctic
Water Inflow Region: Investigated
Through Inverse Modeling.
Front. Mar. Sci. 6:244.
doi: 10.3389/fmars.2019.00244

Kalle Olli^{1,2*}, Elisabeth Halvorsen³, Maria Vernet⁴, Peter J. Lavrentyev^{5,6},
Gayantonia Franzè^{7†}, Marina Sanz-Martin⁸, Maria Lund Paulsen⁹ and Marit Reigstad³

¹ Institute of Agricultural and Environmental Sciences, Estonian University of Life Sciences, Tartu, Estonia, ² Institute of Ecology and Earth Sciences, University of Tartu, Tartu, Estonia, ³ Department of Arctic and Marine Biology, UiT The Arctic University of Norway, Tromsø, Norway, ⁴ Integrative Oceanography Division, Scripps Institution of Oceanography, San Diego, CA, United States, ⁵ Department of Biology, The University of Akron, Akron, OH, United States, ⁶ Department of Zoology, Herzen State Pedagogical University of Russia, Saint Petersburg, Russia, ⁷ Graduate School of Oceanography, University of Rhode Island, Narragansett, RI, United States, ⁸ Department of Global Change Research, Instituto Mediterraneo de Estudios Avanzados (IMEDEA-CSIC-UIB), Esporles, Spain, ⁹ Department of Biological Sciences, University of Bergen, Bergen, Norway

We used inverse modeling to reconstruct major planktonic food web carbon flows in the Atlantic Water inflow, east and north of Svalbard during spring (18–25 May) and summer (9–13 August), 2014. The model was based on three intensively sampled stations during both periods, corresponding to early, peak, and decline phases of a *Phaeocystis* and diatom dominated bloom (May), and flagellates dominated post bloom stages (August). The food web carbon flows were driven by primary production (290–2,850 mg C m⁻² d⁻¹), which was channeled through a network of planktonic compartments, and ultimately respired (180–1200 mg C m⁻² d⁻¹), settled out of the euphotic zone as organic particles (145–530 mg C m⁻² d⁻¹), or accumulated in the water column in various organic pools. The accumulation of dissolved organic carbon was intense (1070 mg C m⁻² d⁻¹) during the early bloom stage, slowed down during the bloom peak (400 mg C m⁻² d⁻¹), and remained low during the rest of the season. The heterotrophic bacteria responded swiftly to the massive release of new DOC by high but decreasing carbon assimilation rates (from 534 to 330 mg C m⁻² d⁻¹) in May. The net bacterial production was low during the early and peak bloom (26–31 mg C m⁻² d⁻¹) but increased in the late and post bloom phases (>50 mg C m⁻² d⁻¹). The heterotrophic nanoflagellates did not respond predictably to the different bloom phases, with relatively modest carbon uptake, 30–170 mg C m⁻² d⁻¹. In contrast, microzooplankton increased food intake from 160 to 380 mg C m⁻² d⁻¹ during the buildup and decline phases, and highly variable carbon intake 46–624 mg C m⁻² d⁻¹, during post bloom phases. Mesozooplankton had an initially high but decreasing carbon uptake in May (220–48 mg C m⁻² d⁻¹), followed by highly variable carbon

consumption during the post bloom stages (40–190 mg C m⁻² d⁻¹). Both, micro- and mesozooplankton shifted from almost pure herbivory (92–97% of total food intake) during the early bloom phase to an herbivorous, detritivorous and carnivorous mixed diet as the season progressed. Our results indicate a temporal decoupling between the microbial and zooplankton dominated heterotrophic carbon flows during the course of the bloom in a highly productive Atlantic gateway to the Arctic Ocean.

Keywords: carbon flow, food web, inverse method, Arctic Ocean, plankton communities

INTRODUCTION

Global ocean annual primary production is declining (Gregg et al., 2003), particularly in the unproductive and expanding oligotrophic gyres (Polovina et al., 2008). The trend is radically different in the Arctic Ocean, where thinning of ice and reduced ice cover (Stroeve and Notz, 2018) drive a spectacular trend toward increased phytoplankton surface concentrations and primary production (Arrigo and van Dijken, 2015; Kahru et al., 2016; Hill et al., 2018).

Climate warming is especially severe in the Arctic, where the average temperature is increasing 0.4°C per decade, several times higher than the global average rate (Stocker, 2014). The Arctic has lost more than half of its summer ice extent since 1980, and predictions suggest that the Arctic Ocean will be ice free in the summer as early as 2050 (González-Eguino et al., 2017). This could further accelerate the Arctic amplification through enhanced sea–ice–albedo feedback, leading to a self-accelerating vicious warming cycle (Graversen et al., 2008; Kashiwase et al., 2017). The net effect is increasing primary production due to longer open water productive seasons and adaptation of algal bloom patterns to earlier melting and later freeze up (Arrigo and van Dijken, 2015).

The European Arctic Ocean (Barents Sea and the Fram Strait) is highly influenced by the warm Atlantic water brought by the North Atlantic Current, causing it to be a relatively ice free area, and introducing also nutrient-rich waters as well as non-indigenous Atlantic species and living biomass (Chan et al., 2018; Neukermans et al., 2018). The effect and fate of this advected biomass is not clear. The nutrients transported may become available for primary production through upwelling events, creating hotspots of increased productivity along the shelf breaks (Tremblay et al., 2011). The region north of Svalbard is projected to become a new productive hot spot in the Arctic Ocean due to the ice retreat.

The inflow of Atlantic water from the North Atlantic Current and the West Spitsbergen Current along the eastern Fram Strait has intensified over recent decades (Beszczynska-Moller et al., 2012). Further, the long-term environmental monitoring revealed a 1°C higher warm water anomaly event in the Atlantic Water inflow from 2005 to 2007, accompanied with shifts in dominant phytoplankton species in summer from large-celled diatoms to smaller flagellates like coccolithophorides and *Phaeocystis*, a change which appeared persistent also after the reversal of the temperature anomaly (Nöthig et al., 2015). These changes at the primary producers level cascaded further into the food web,

where mesozooplankton adapted by shifting from predominantly herbivory to omnivory and detritivory (Vernet et al., 2017).

The pelagic microbial food webs in the Arctic Ocean are commonly described to have distinct community structure and low diversity, with essentially no cyanobacteria, and high levels of endemism (Lovejoy et al., 2006; Pedrós-Alió et al., 2015). The fate and partitioning of the enhanced primary production in the arctic pelagic food web is still largely unknown and only a few field studies exist (Vézina et al., 2000; Forest et al., 2011; Tremblay et al., 2012; Saint-Béat et al., 2018). Food web integrates the transfer of matter and energy between organisms that eat, and are eaten by others, capturing thus essential information about species interactions, material flow, community structure, and ecosystem functioning. The seasonal progression of community maturation is reflected in food web reorganization, which can cause changes in ecosystem performance (Samhuri et al., 2009; Blais et al., 2017).

Here, we use linear inverse modeling (Vézina and Platt, 1988; Vézina et al., 2000; De Laender et al., 2010; van Oevelen et al., 2010) to resolve and quantify food web trophic flows of organic carbon between major planktonic components in the Atlantic Water inflow to the Arctic Ocean during cruises in early and later summer seasons of 2014. Since the pivotal text by Vézina and Platt (1988), the inverse method has become increasingly popular in aquatic food web modeling. It enables estimating elemental budgets and reconstructing otherwise notoriously difficult to measure trophic flows between living compartments, using the relatively easy to measure biomasses of these compartments; a set of measured flows (e.g., primary production and respiration), food web topology, and biologically meaningful constraints on the trophic flows (De Laender et al., 2010). The methodology has been used to quantify planktonic food web flows in natural and experimental systems (Vézina et al., 2000; Olsen et al., 2006; Luong et al., 2014), has been used to track biogenic carbon flow in the Arctic (Vézina et al., 2000; Forest et al., 2011; Vernet et al., 2017), and last but not least, is coded in open source software (*LIM* library of the R software) with good explanatory texts (Soetaert and van Oevelen, 2009; van Oevelen et al., 2010).

The goal of the 2014 summer cruises was to map the physical and biogeochemical properties of the Atlantic Water inflow to the Arctic Ocean. Our synthesis relies on *in situ* data on phytoplankton particulate and dissolved production, bacterial production, community respiration, vertical particle fluxes, and pools of particulate and dissolved organic carbon. The model provides information on the trophic interaction,

assimilation and exudation rates that may regulate the organic carbon export partitioning between the respiration and biological carbon pump.

MATERIALS AND METHODS

Spatial Coverage and Water Column Profiles

Data were collected during two cruises on board the R/V Helmer Hanssen, on and off the shelf northwest and north of Svalbard. Three 24 h process stations were sampled in May, corresponding to early, peak, and decline phase of an algal bloom, and three stations in August, representing post bloom stages (Figure 1 and Table 1). Sampling stations were located to intercept the core of the warm Atlantic water inflow, which enters the Arctic Ocean with the West Spitsbergen Current east and north of Svalbard (Randelhoff et al., 2018).

Vertical profiles of temperature, salinity and fluorescence were mapped with a rosette oceanographic profiler (CTD, Seabird SBE 911 plus). Water for analysis of carbon pools and biological process studies was retrieved with 5 L Niskin bottles from discrete depths (1, 5, 10, 20, 30, 40, 50, 75, 100, and 200 m), and the fluorescence maximum.

Carbon Pools

Total chlorophyll *a* (Chl *a*) samples (100–150 ml) were filtered onto Whatman GF/F glass-fiber filters (nominal pore of 0.7 μm).

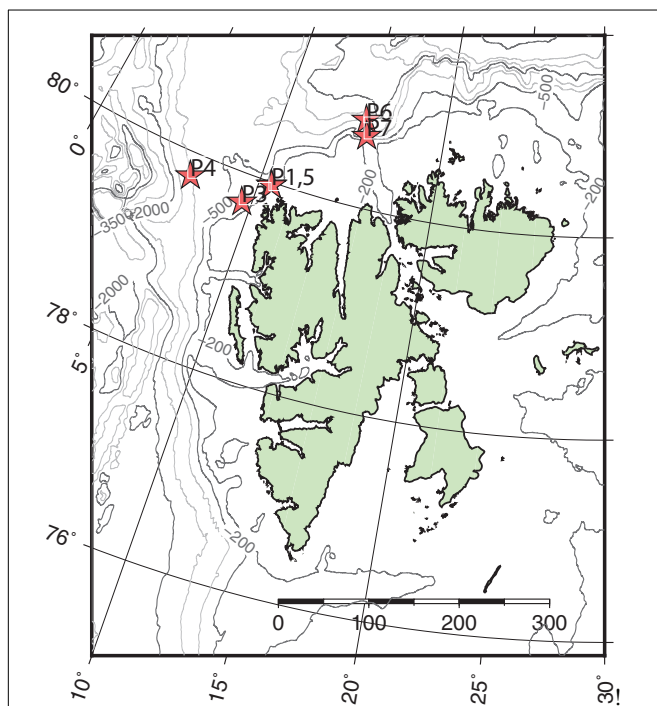


FIGURE 1 | Chart of the research area around Svalbard, with sampling stations during the two cruises in May (P1–P4) and August (P5–P7). Locations of P1 and P5 coincide. P2 is missing due to lost moorings. Scale bar in km.

TABLE 1 | Location of 24 h process stations in May and August 2014.

Stn	Date	Lat (°N)	Lon (°E)	d_{ML} (m)	Z_{eu} (m)	Bloom stage
P1	May 18	79.975	10.709	10	23	Early
P3	May 23	79.718	9.457	10	19	Peak
P4	May 25	79.771	6.270	11	22	Late
P5	August 09	79.970	10.725	15	22	Post
P6	August 11	80.860	15.002	10	48	Post
P7	August 13	80.706	15.266	9	45	Post

Depths of the mixed layer (d_{ML}) and photic zone (Z_{eu}) at each station according to Randelhoff et al. (2018). Mixed layer is defined as the depth where MSS-90L microstructure sonde measured potential density (σ_θ) crosses 20% of the density difference between a surface layer density (3–5 m), and deeper (reference depth interval 50–60 m). Photic zone is defined as the depth where downwelling PAR reached 1% surface value. The phytoplankton bloom stage according to Reigstad et al. (in preparation). Stn P2 is missing due to loss of moorings carrying primary production incubations and sediment traps.

In addition, size fractionated Chl *a* (>10 μm , <3 μm) was obtained with membrane filters. Chl *a* was extracted in 5 ml of methanol at room temperature in the dark for 12 h without grinding. Triplicate samples of each size fraction were read with a Turner Fluorometer AU-10 (Holm-Hansen et al., 1965). Size-fractionated Chl *a* biomass was converted into phytoplankton carbon using a conversion factor of 27 (Riemann et al., 1989).

Total organic carbon (TOC) was measured from unfiltered seawater by high temperature combustion using a Shimadzu TOC-VCSH. Samples were acidified with HCl (to a pH of around 2) and bubbled with N_2 gas in order to remove inorganic carbon. Particulate organic carbon (POC) samples were filtered in triplicate (100–500 ml) onto pre-combusted Whatman GF/F (450°C for 5 h), dried at 60°C for 24 h and analyzed on-shore with a Leeman Lab CEC 440 CHN analyzer after removal of carbonate with fumes of concentrated HCl for 24 h (Fischer and Wefer, 2013).

The concentration of dissolved organic carbon (DOC) was calculated from the difference of TOC and POC.

Heterotrophic bacteria (BAC) and heterotrophic nanoflagellates (HNF) were counted on an Attune[®] Focusing Flow Cytometer (Applied Biosystems by Life Technologies) with a syringe-based fluidic system and a 20 mW 488 nm (blue) laser. Samples were fixed with glutaraldehyde (0.5% final conc.) at 4°C for a minimum of 2 h, shock frozen in liquid nitrogen, and stored at –80°C until analysis. For enumeration of bacteria the samples were diluted 10-fold with 0.2 μm filtered TE buffer (Tris 10 mM, EDTA 1 mM, pH 8), stained with a green fluorescent nucleic-acid dye, SYBR Green I (Molecular Probes Inc., Eugene, OR, United States) and kept for 10 min at 80°C. HNF samples were preserved in similar way, following staining with SYBR Green I (Molecular Probes Inc., Eugene, OR, United States) for 2 h in the dark, and minimum 1 ml was measured at a flow rate of 500 $\mu\text{l min}^{-1}$ (Zubkov et al., 2007). HNF were discriminated from nano-sized phytoplankton on basis of green vs. red fluorescence, and from large bacteria on basis of side scatter vs. green fluorescence. Abundances were converted to carbon biomass using a bacterial carbon

content of 15 fg C cell⁻¹, and a HNF mean cell size of 33.5 μm³ and 20% carbon content (Børsheim and Bratbak, 1987; Ducklow, 2000).

Microzooplankton samples were preserved in 2% (final concentration) acid Lugol's iodine, post-fixed with 1% (final concentration) formaldehyde after 24 h and stored at 4°C until counting. Microzooplankton were settled in Utermöhl chambers (50–100 ml) and counted under differential interference contrast (DIC) and fluorescence equipped inverted microscope. The entire chamber was scanned at 200× magnification. At least 40 individual cells within each abundant taxon were sized at 400–600× magnification and converted to carbon biomass according to geometric shapes and volume to carbon conversions (Menden-Deuer and Lessard, 2000). All ciliates, and hetero- and mixotrophic dinoflagellates > 20 μm in maximum dimension were allocated to microzooplankton.

Mesozooplankton composition, biomass, and depth distribution was assessed with net hauls from the bottom (or a maximum depth of 1,000 m at station deeper than 1,000 m) to the surface twice a day (noon and midnight). The vertically stratified samples (0–20, 20–50, 50–100, 100–200, 200–600, and 600–1,000 m) were collected with a MultiNet Midi (180 μm mesh size, 0.25 m² mouth opening, Hydro-Bios, Kiel, Germany) that was deployed vertically with a hauling speed of 0.5 m s⁻¹. Samples were preserved in a solution of 80% seawater and 20% fixation agent (75% formaldehyde buffered with hexamine, 25% anti-bactericide propandiol), resulting in a final formaldehyde concentration of 4% (for details see: Basedow et al., 2018).

From the fixed samples, zooplankton was counted and identified to the level of species (most copepods), genus or family (other groups). Conspicuous, large zooplankton (> 5 mm, chaetognaths > 10 mm) were identified and enumerated from the entire sample. From the rest of the sample, at least 500 individuals from a minimum of three sub samples (2 ml, obtained with an automatic pipette with tip end cut to leave a 5 mm opening) were identified, staged and counted. This procedure allows for the analysis of abundance of common species and taxa with 10% precision and at 95% confidence level (Postel et al., 2000). Copepods of the genus *Calanus* were identified to species level (Kwasniewski, 2003). Specimens other than copepods were measured and sorted into different size categories. For the inverse reconstruction, mesozooplankton was aggregated into two size classes, small (<4 mm), and large (>4 mm). The latter also included the *Calanus* species (*Calanus finmarchicus*, *Calanus glacialis*, and *Calanus hyperboreus*). Mesozooplankton abundance was converted to carbon biomass by using species-specific conversion factors after an extensive compilation (E. Halvorsen, unpublished data) from a range of literature sources (e.g., Richter, 1994; Hanssen, 1997; Hirche and Kosobokova, 2003; Hopcroft et al., 2010), or a generic biovolume to carbon conversion factor of 0.03 mg C mm⁻³ (Zhou et al., 2010).

Community Metabolic Rates

Algal ¹⁴CO₂ fixation was measured by the ¹⁴C method (Nielsen, 1952). Water samples from 1, 5, 10, 20, 30, 40, 50, and 75 m depth were split in 100 ml aliquots into four 150 ml polycarbonate

bottles and spiked with 10 μCi of NaH¹⁴CO₃. One bottle served as a t₀ sample. One dark, and duplicate light bottles were incubated at *in situ* depths for ca 22 h, using a freely drifting or ice-floe attached mooring. Total ¹⁴CO₂ fixation, including organic exudates, was measured from a 2 ml sub-sample, and particulate ¹⁴CO₂ fixation from the remaining 98 ml Whatman GF/F filtered sample, placed in 6 ml scintillation vials. Residues of any inorganic ¹⁴C were removed by acidifying the samples with 0.2 ml of 20% HCl for 24 h. After acidification, 5 ml of Ultima GoldTM XR LSC scintillation cocktail was added, and the samples stored in the dark until measuring on shore in a PerkinElmer Tri-Carb 2900TR scintillation counter. The activity in dark bottle was subtracted from the activities in the light bottles, and to assess dissolved primary production the particulate primary production was subtracted from the total. The detection limit was approximately 1 μg C L⁻¹ d⁻¹. In our study the ¹⁴CO₂ fixation rates were treated as gross primary production (GPP).

Bacterial production (BP) was measured using the radio-labeled leucine incorporation technique (Kirchman, 2001). Aliquots of 1.9 ml were incubated with ³H-leucine (final conc. 20 nmol L⁻¹; specific activity 5.957 TBq mmo L⁻¹) in the dark at 1°C for 2 h. Triplicate samples were taken from each profile depth, as well as one trichloroacetic acid (TCA) killed control (5% final concentration). The reaction was terminated by adding TCA (5% final concentration). Samples were microcentrifuged and aspirated. The remaining pellet was subsequently washed with TCA and ethanol. The samples were dried, and radio assayed with scintillation cocktail (Ultima GoldTM XR LSC) with a PerkinElmer Tri-Carb 2900TR scintillation counter. Bacterial carbon production was calculated with a conversion factor 3.1 kg C mol⁻¹ leucine incorporated (Simon and Azam, 1989).

Community respiration (ComResp) was determined from changes in oxygen over a 24 h period in 100 ml sample aliquots. Oxygen concentrations were analyzed by micro-Winkler titration using a potentiometric electrode and automated endpoint detection (Mettler Toledo, DL28 titrator) following Oudot et al. (1988). Community respiration was calculated by subtracting initial dissolved oxygen concentrations from dissolved oxygen concentrations measured after incubation in the dark. Due to the small aliquot volume, it was unlikely to contain any representative quantity of mesozooplankton. Therefore, the community respiration was not partitioned to mesozooplankton in the inverse reconstruction.

Vertical Particle Flux

To measure the vertical flux of organic particles (SED), we deployed a drifting, semi-Lagrangian array of sediment traps at eight depths (20, 30, 40, 50, 60, 90, 120, and 200 m). The array was free drifting or attached to an ice floe and was deployed for ca. 24 h. The sediment traps were parallel cylinders (7.2 cm in diameter, 45 cm height) mounted in a gimbaled frame equipped with a vane. At moderate current speeds, the cylinders remain vertical and perpendicular to the current direction. No baffles were used in the cylinders opening, and no fixatives were added to the traps prior to deployment. After recovery, the contents of the two replicate sediment trap cylinders were pooled into

plastic bottles and kept cold and dark until processing for POC as described above.

Inverse Model Specification

To estimate the carbon flows between food web compartments with the linear inverse model (LIM), we need food web topology (matrix E), the measured compartment biomasses and rates of change therein ($\Delta\text{biomass}/\Delta t$; vector f), and a set of quantitative constraints. The constraints can be directly measured by flows of the food web (hard constraints), or plausible physiological properties usually based on a literature search, which set the upper or lower bounds of flows (weak constraints). E.g., it is reasonable to consider all food web flows to be non-negative. The web topology (matrix E) describes the mass balances of the compartments, i.e., the flows of mass in and out of pre-defined compartments and is constructed based on our understanding of trophic relationships (who eats what). There are as many columns in matrix E as there are flows in the food web, and as many rows as there are compartments. The E matrix and f vector combined obey the conservation of mass principle, i.e., the compartment mass change equals to the sum of flows in, minus the sum of flows out of the compartment. Each compartment has its own mass balance equation, with unknown food web flow values. To solve the inverse problem, we need to find the unknown food web flows, forming a solution vector x , which simultaneously satisfies all the mass balances equations. In a matrix format the system of linear equations to be solved is:

$$E^*x = f$$

where matrix E is made of the coefficients in the mass balance equation, the solution vector x has a length equal to the number of columns in E , and the compartment mass change vector f has a length equal to the rows of E . Further, the solution vector has to satisfy a set of quantitative constraints. If some of the food web flows, or combination of flows, are measured from the food web under study (hard constraints), we constrain that flow,

or combination of flows, to a particular value, which the solution vector has to satisfy. Each measured flow adds another equation to the system of linear equations. The solution vector also has to satisfy weak constraints (coefficients in matrix G), which set the upper or lower limits (vector h) to certain food web flows:

$$G^*x \geq h$$

E.g., food assimilation cannot be more than food intake by the organisms. Unlike more conventional modeling, which is a predictive tool to forecast changes in standing stocks form a set of deduced properties, inverse modeling does not predict, but inversely back-calculates the properties from observed data and plausible constraints.

In our study we grouped the pelagic food web components into 10 compartments, eight living and two non-living, for which mass balance equations were constructed (**Supplementary Table S1**). The eight living compartments of organism groups comprised the three size classes of autotrophs (PHY0, <3 μm ; PHY1, 3–10 μm ; PHY2, >10 μm , containing also the colonial *Phaeocystis*), heterotrophic bacteria (BAC), heterotrophic nanoflagellates enumerated with flow-cytometry (HNF), microzooplankton (μZOO), and two size classes of mesozooplankton (ZOO1, ZOO2; **Table 2**). The two non-living compartments were dissolved organic carbon (DOC) and detritus (DET, derived from measured POC minus the carbon biomass of living compartments). All compartments were expressed in units of organic carbon (mg C m^{-3}), and for the inverse reconstruction integrated to the upper 40 m layer (mg C m^{-2}). The upper 40 m layer included the surface mixed layer, and in most cases the euphotic layer (**Table 1**).

The inverse model had three external flows: (i) primary production (GPP), fueling new organic carbon into the food web, and two flows by which carbon left the food web, (ii) respiration, and (iii) sedimentation of organic particles (SED). The model was driven by primary production, measured at each station,

TABLE 2 | Abbreviations of the planktonic food web compartments, the respective stock sizes (mg C m^{-2}) in the upper 40 m water column, and changes of stocks ($\text{mg C m}^{-2}\text{d}^{-1}$) in stations P1–P7.

Comp	P1	P3	P4	P5	P6	P7
PHY0	1350 (+186)	3070 (+24)	593 (–71)	1490 (+108)	364 (–158)	604 (+165)
PHY1	670 (–40)	1100 (–53)	1280 (–60)	327 (+19)	187 (–100)	268 (+103)
PHY2	5020 (+150)	7540 (+6)	4300 (–93)	388 (–1.6)	453 (–137)	598 (+112)
ΣP	7040 (+295)	11700 (–23)	6170 (–225)	2200 (–125)	1000 (–396)	1470 (+380)
BAC	437 (+8.7)	803 (–6.8)	867 (–59)	655 (+7.3)	509 (–168)	856 (+34)
HNF	100 (+38)	357 (–30)	613 (–91)	368 (+4.6)	287 (–139)	224 (+1.7)
μZOO	261 (+37)	418 (–23)	238 (–54)	944 (+4.6)	761 (–139)	910 (–28)
ZOO1	311 (+26)	124 (+9.0)	81 (+0.7)	149 (+13)	214 (+0.4)	382 (+35)
ZOO2	633 (+24)	627 (+4.6)	843 (+1.7)	364 (+7.7)	593 (+1.2)	800 (+27)
ΣZ	1310 (+125)	1530 (–40)	1780 (–143)	1830 (+30)	1860 (–276)	2320 (+36)
DET	220 (+80)	4430 (–11)	6670 (–81)	4220 (+9.3)	3720 (–122)	3260 (+66)
DOC	28500 (+1071)	31300 (+399)	25500 (+79)	29900 (+62)	28400 (–150)	29200 (+20)

PHY0, pico autotrophs < 3 μm ; PHY1, nano autotrophs 3–10 μm ; PHY2, micro autotrophs > 10 μm , including colonial *Phaeocystis*; BAC, heterotrophic bacteria; HNF, heterotrophic nanoflagellates; μZOO , microzooplankton (ciliates and heterotrophic dinoflagellates); ZOO1, mesozooplankton < 4 mm; ZOO2, mesozooplankton > 4 mm (inc. *Calanus spp.*); DET, detritus; DOC, dissolved organic carbon. ΣP , sum of phototrophs; ΣZ , sum of grazers (HNF + μZOO + ZOO1 + ZOO2).

and integrated vertically to 40 m depth through trapezoidal integration ($\text{mg C m}^{-2} \text{d}^{-1}$).

The measured community respiration (ComResp) was the sum of respiration by all living compartments (three size classes of phytoplankton, bacteria, heterotrophic nanoflagellates, and microzooplankton), with the exception of mesozooplankton. Community respiration measurements were conducted from the upper mixed layer, intermediate layer and chlorophyll maximum, and integrated vertically through trapezoidal integration ($\text{mg C m}^{-2} \text{d}^{-1}$), assuming 1:1 ratio (O:C).

Sedimentation of organic particles was measured as POC ($\text{mg POC m}^{-2} \text{d}^{-1}$) and partitioned by the food web model between three compartments: detritus (DET), large phytoplankton (PHY2), and mesozooplankton fecal pellets.

All three phototrophic compartments acquired CO_2 for photosynthesis, incorporated part of organic carbon as biomass (measured as particulate primary production), and exuded part of the organic carbon to the DOC pool (measured as dissolved primary production), and part of the carbon was respired back to CO_2 . A fraction of the phototrophic biomass was lost to detritus through processes like mortality and lysis. Only the largest phytoplankton fraction (PHY2) contributed directly to sinking particles; smaller phytoplankton fractions contributed to vertical flux indirectly through detritus.

Bacteria took up DOC from the environment (bacterial assimilation), part of it was respired to CO_2 , and part was incorporated into biomass (measured as net bacterial production). Bacterial biomass was lost to detritus through mortality. Viral lysis of bacteria can release significant amount of DOC also in high latitude marine environments (Chénard and Lauro, 2017), which is again taken up by the bacterial community. This viral loop and other causes of inter-bacterial DOC cycling are not dealt with explicitly here and are all incorporated into the bacterial compartment in our model.

Heterotrophic nanoflagellates and microzooplankton fed on smaller living compartments, microzooplankton also on detritus, and lost biomass through respiration to CO_2 , exudation of organic matter to DOC, mortality to detritus, and through grazing by larger organisms. Microzooplankton, composed of heterotrophic dinoflagellates and ciliates in our study, are known grazers on *Phaeocystis* (Grattepanche et al., 2011; Swalethorp et al., 2019), but the grazing pressure depends on whether the prymnesiophyte is in its single-cell or colonial form (Grattepanche et al., 2011). Further, heterotrophic dinoflagellates are known to be voracious predators of large phytoplankton like other dinoflagellates and diatoms (Olseng et al., 2002; Jeong et al., 2004). We therefore allowed microzooplankton to prey on all size classes of phototrophs. We are also aware that several microzooplankton taxa could be mixotrophic, as kleptoplasty is common in both, dinoflagellates and ciliates (Gast et al., 2007; Stoecker et al., 2009), but these pathways are currently not considered in our model.

Mesozooplankton grazed on detritus and all other heterotrophic and phototrophic compartments except bacteria, picophototrophs, and large mesozooplankton also nano phototrophs. Mesozooplankton lost biomass through DOC release (sloppy feeding and other processes), respiration, and

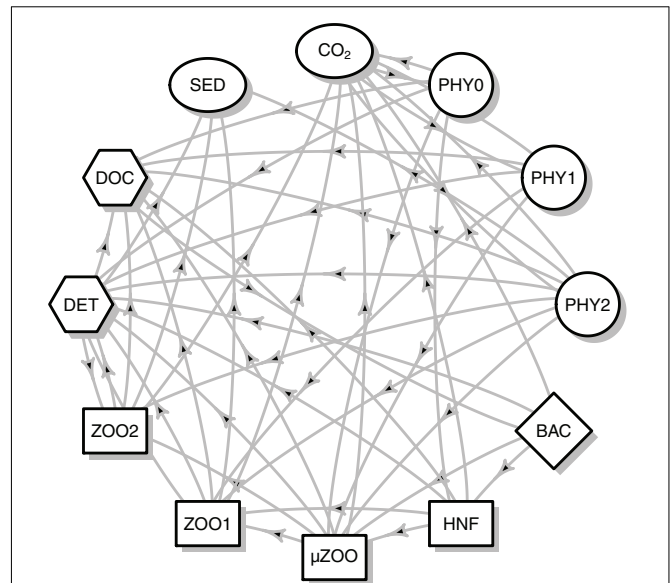


FIGURE 2 | Food web topology of the linear inverse models. The same topology was used for all stations. Arrows represent carbon flows between compartments. Autotrophic compartments are in circle: PHY0, pico autotrophs < 3 μm ; PHY1, nano autotrophs 3–10 μm ; PHY2, micro autotrophs > 10 μm including colonial *Phaeocystis*. Diamond: BAC, heterotrophic bacteria; Heterotrophic grazers are in rectangles: HNF, heterotrophic nanoflagellates; μZOO , microzooplankton; ZOO1, small mesozooplankton < 4 mm; ZOO2, large mesozooplankton > 4 mm; Non-living organic compartments are in hexagons: DOC, dissolved organic carbon; DET, detritus. External compartments, with no mass balance equations, are in ellipses: SED, sedimentary carbon; CO_2 , respired carbon.

defecation. Part of the feces contributed directly to sinking particles, the other part disintegrated in the water column and contributed to the detritus pool (Wexels Riser et al., 2002). The detritus compartment gained biomass through mortality of all living compartments, and lost biomass to DOC through bacterial and chemical degradation, and through sedimentation.

The food web topology, showing all the linkages between compartments, is outlined in **Figure 2**. To narrow the allowable ranges for the reconstructed food web flows, we set an array of biologically relevant constraints (**Supplementary Table S2**). All flows were expected to be non-negative. The particulate and dissolved primary production was partitioned between the three phototrophic size classes according to the respective biomasses, but allowing for allometric negative scaling between cell size and mass-specific photosynthesis rate (Maraóón et al., 2007). We thus constrained the mass-specific primary production for smaller autotrophs to be larger than for the subsequent large autotroph compartment, but not more than two times larger. Autotrophic respiration was constrained to between 1 and 55% of the gross primary production (Falkowski et al., 1985). Phytoplankton mortality was assumed to be at least 1% of the biomass per day.

For mesozooplankton we constrained the assimilation to be 40–80% of the food intake (Parsons et al., 2014). For other heterotrophic grazers (HNF, μZOO) the assimilation was assumed to be 80–90% of the food intake (Straile, 1997). Bacterial

assimilation efficiency was assumed to be 100%. Respiration of the heterotrophic compartments was partitioned into a maintenance respiration, constrained between 1 and 10% of their respective biomass, and respiration associated with growth, which was constrained to be at least 40% of the assimilated food for eukaryotes (Sanders et al., 1992), or at least 10% for bacteria (del Giorgio and Cole, 1998).

Mesozooplankton DOC release (sloppy feeding, other processes) was constrained to be between 1 and 50% of the food intake (Møller et al., 2003; Møller, 2004). Mesozooplankton defecation was constrained between 10 and 60% of the food intake, and was further partitioned into a vertical particle flux of rapidly sinking fecal pellets, and disintegration within the water column into the detritus pool (Wexels Riser et al., 2002). Further, the fraction of sinking fecal pellets was set to be less than the flow to detritus pool, to be consistent with field observations from the Barents Sea (Wexels Riser et al., 2002). Microzooplankton and heterotrophic nanoflagellate exudation to DOC pool was constrained between 1 and 10% of food intake, and mortality between 1 and 10% of biomass per day. Bacterial daily mortality was set to be 1–10% of the bacterial biomass.

If heterotrophic grazers did not discriminate between food sources, the grazing rates would be proportional to the biomass of the respective prey items. We allowed preferential grazing and some discrimination between food sources, but not more than 0.5–2.0 times the respective prey biomass ratios. Further, we assumed that zooplankton grazers (μ ZOO, ZOO1, and ZOO2) feed on both, living compartments and detritus, but that they prefer living prey. Therefore, the grazing rates on detritus divided by the grazing rates on live compartments was set lower than the biomass ratio of detritus to live prey compartments.

In summary, the inverse food web model had 10 compartments with mass balances (eight living, two non-living; **Figure 2** and **Supplementary Table S1**), five measured flows (community respiration, particulate and dissolved primary productions, bacterial net production, vertical flux of organic particles), 48 reconstructed food web flows (**Figure 2** and **Supplementary Table S3**), and 85 biological constraints (**Supplementary Table S2**). The inverse reconstruction was run with the LIM library of the R software (van Oevelen et al., 2010). The food web architecture and biological constraints were kept constant throughout the study and were applied for each individual data set from stations P1–P7. With 15 equations (10 mass balances plus 5 measured flows) and 48 unknown flows (rank parameter equal to 15), the system was under-determined and had infinite number of solutions, which satisfy the equations. A sensible choice is to follow the principle of parsimony, picking a solution with the minimum norm, i.e., the solution with the lowest sum of squared flow values.

However, this minimum norm solution is not based on ecological theory nor supported by empirical evidence. Further, it tends to push some of the flows to the lower bounds of their possible ranges, which should be considered extreme rather than likely values (Kones et al., 2006). We therefore opted here for the alternative likelihood approach, which considers all the possible solutions of the food web by sampling the probability density function (PDF) of LIM solution space by using a Markov Chain

Monte Carlo algorithm (Meersche et al., 2009). This approach has an interesting useful property: although the PDF of the LIM domain is uniform, emphasizing that all valid solutions are equally likely, the marginal probability density function (mPDF) of an individual flow is not uniform. This is because mPDF integrates over the valid areas of all other flows and therefore some selections within the individual flow range render as more likely (van Oevelen et al., 2010). We fed the *xsample()* function with initial minimum norm solution [obtained with function *lsei()*] as an initial starting set and sampled the LIM solution space with 10,000 MCMC random draws. The *xsample()* MCMC algorithm uses a symmetrical random jump function that only depends on the previously accepted point to draw a new sample. Each of the realizations corresponds to an equally likely solution vector x of the food web flows, which obeys the mass balances, as well as the data and constraints. Here we summarize the likelihood of each individual flow as the mean (\pm SD) of the sampled mPDF.

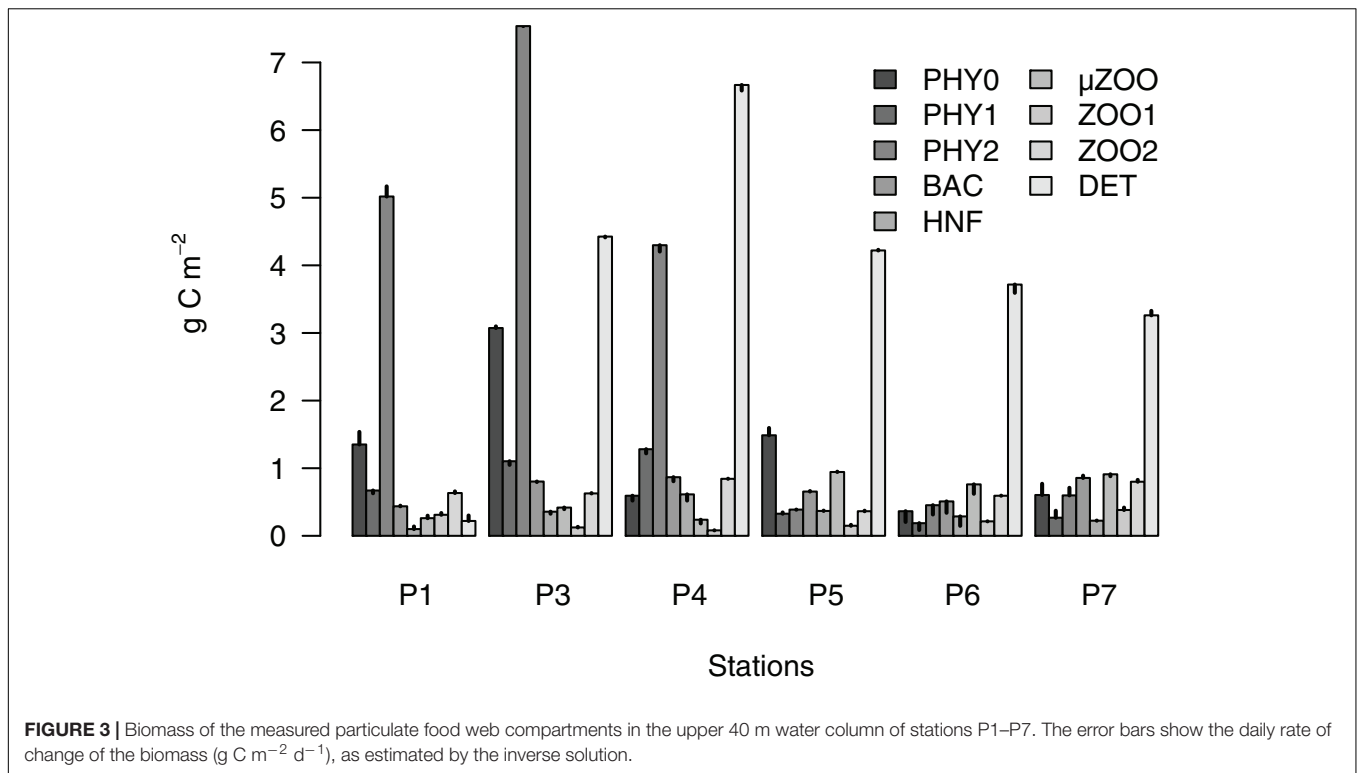
The mass balance equations are usually balanced with rates of change of the compartment biomasses, measured over a period of time (e.g., Forest et al., 2011). In our 24 h process stations no sensible time series was feasible, leaving us with an alternative to assume a steady state food web and consider the rates of biomass change to be zero. However, our measured boundary input flows (primary production) were not balanced by output boundary flows (community respiration plus sedimentation), thus rendering a steady state problem infeasible, unless we introduce new *ad hoc* export or advection functions. To balance the system, we relaxed the steady state assumption, and defined the compartment mass balances as *approximate*, not as *exact* equations in the inverse analysis *lsei()* function, which then resolved the biomass changes in the minimum norm sense. This initial minimum norm solution was then inserted as the starting set to the *xsample()* function (see above).

RESULTS

Measured Biomasses

The measured organic carbon masses of the living and non-living compartments, and their reconstructed rates of change, are given in **Table 2**. The raw vertical profiles of biomasses and flows are presented in **Supplementary Figures S1–S5**. The largest organic carbon pool was in the dissolved fraction (25–31 g C m⁻²). DOC exceeded the particulate carbon pool generally by a factor of 3–4, but only by a factor of 1.6–1.7 during the peak and decline phases of the algal bloom (P3 and P4).

The partitioning of the particulate organic carbon revealed a conspicuous and rapid shift from phytoplankton to detritus domination, as the season progressed (**Figure 3**). The early bloom stage had a very low detritus biomass (ca 0.2 g C m⁻²), but a substantial phytoplankton biomass (>7 g C m⁻²), mostly in the larger micro fraction (5 g C m⁻²). By the peak of the bloom the phytoplankton biomass had increased further (up to ca 12 g C m⁻²; mainly in the micro and pico fractions), but there was also a substantial build-up of detritus (up to 4.4 g C m⁻²). By the late bloom stage, the detritus biomass



reached its peak (ca. 6.7 g C m^{-2}), while the phytoplankton was on decline (6.2 g C m^{-2}). The bloom progression in May followed a shift from *Phaeocystis pouchetii* dominance to a co-dominance with guild of diatoms from the genera *Chaetoceros* (*Chaetoceros socialis*, *Chaetoceros holsaticus*, and *Chaetoceros furcellatus*), *Thalassiosira* (*Thalassiosira hyaline* and *Thalassiosira nordenskiöldii*), *Fragillariopsis* (*Fragillariopsis oceanica* and *Fragillariopsis furcellatus*), and the presence of medium-sized dinoflagellates from the genera *Gymnodinium* and *Protoperidinium*. The post bloom stages in August had only a modest phytoplankton biomass ($1\text{--}2 \text{ g C m}^{-2}$), but the detritus remained high ($3.2\text{--}4.2 \text{ g C m}^{-2}$). Overall the percentage of detritus from POC increased from 2.4 to 24% to 43%, as the bloom progressed in May and varied between 41 and 52% in August. The dominant phytoplankton groups in August were small flagellates, coccolithophorids, cryptophytes, (*Teleaulax*) chrysophytes (*Dinobryon*), chlorophytes (*Pyraminonas*), dinoflagellated (*Gymnodinium* and *Oxyrrhis*), but also some diatoms and *Phaeocystis pouchetii*.

The lower food web components followed the evolution of the successional stages (Table 2). Bacterial biomass doubled from the early to peak and late bloom phases (from 440 to 870 mg C m^{-2}) and remained high during the post bloom stages ($510\text{--}860 \text{ mg C m}^{-2}$). Heterotrophic nanoflagellates revealed a rapid biomass increase from early to late bloom ($100\text{--}610 \text{ mg C m}^{-2}$) and retained a modest biomass during post bloom stages ($220\text{--}370 \text{ mg C m}^{-2}$). Microzooplankton retained low biomass during all the bloom stages ($240\text{--}420 \text{ mg C m}^{-2}$) but increased notably during the post bloom stages ($760\text{--}940 \text{ mg C m}^{-2}$). Mesozooplankton biomass

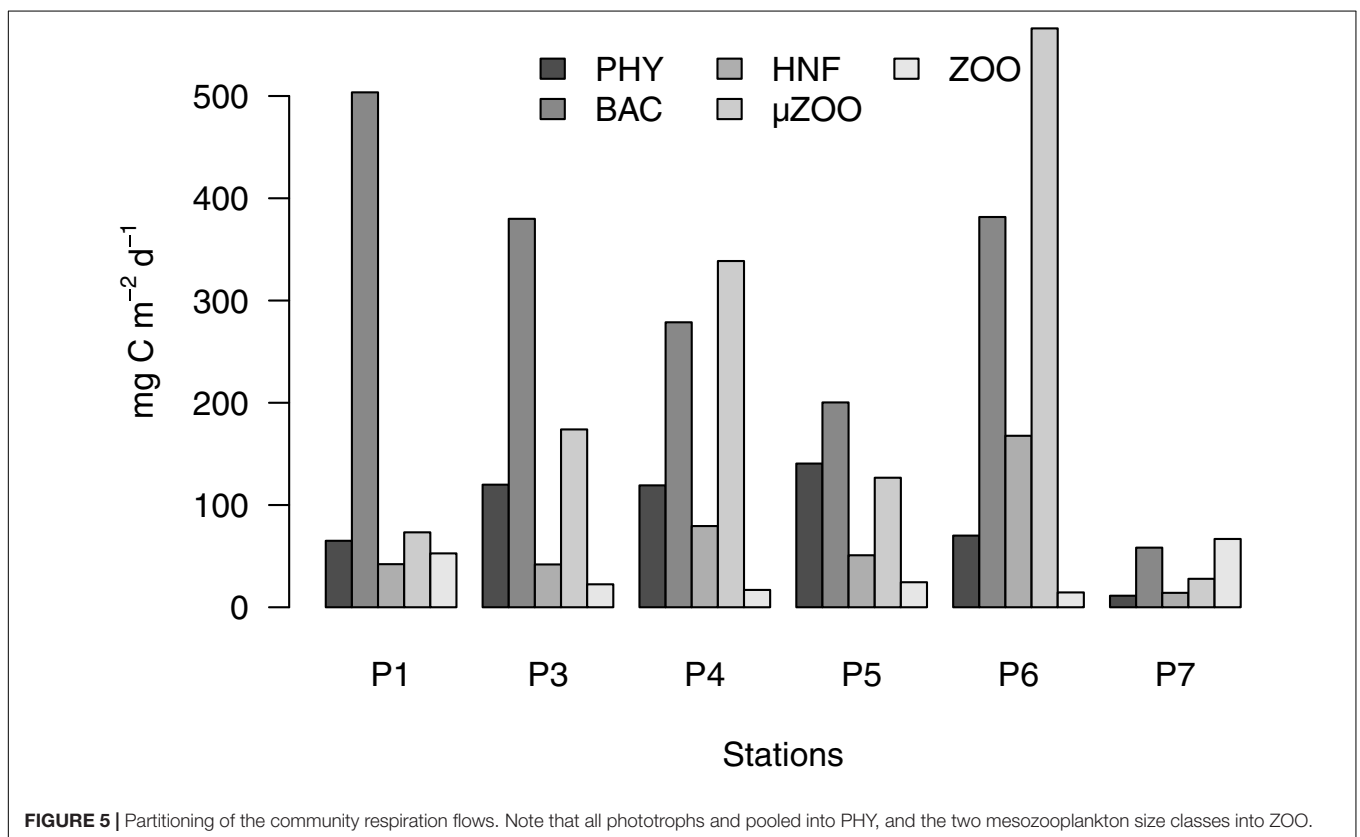
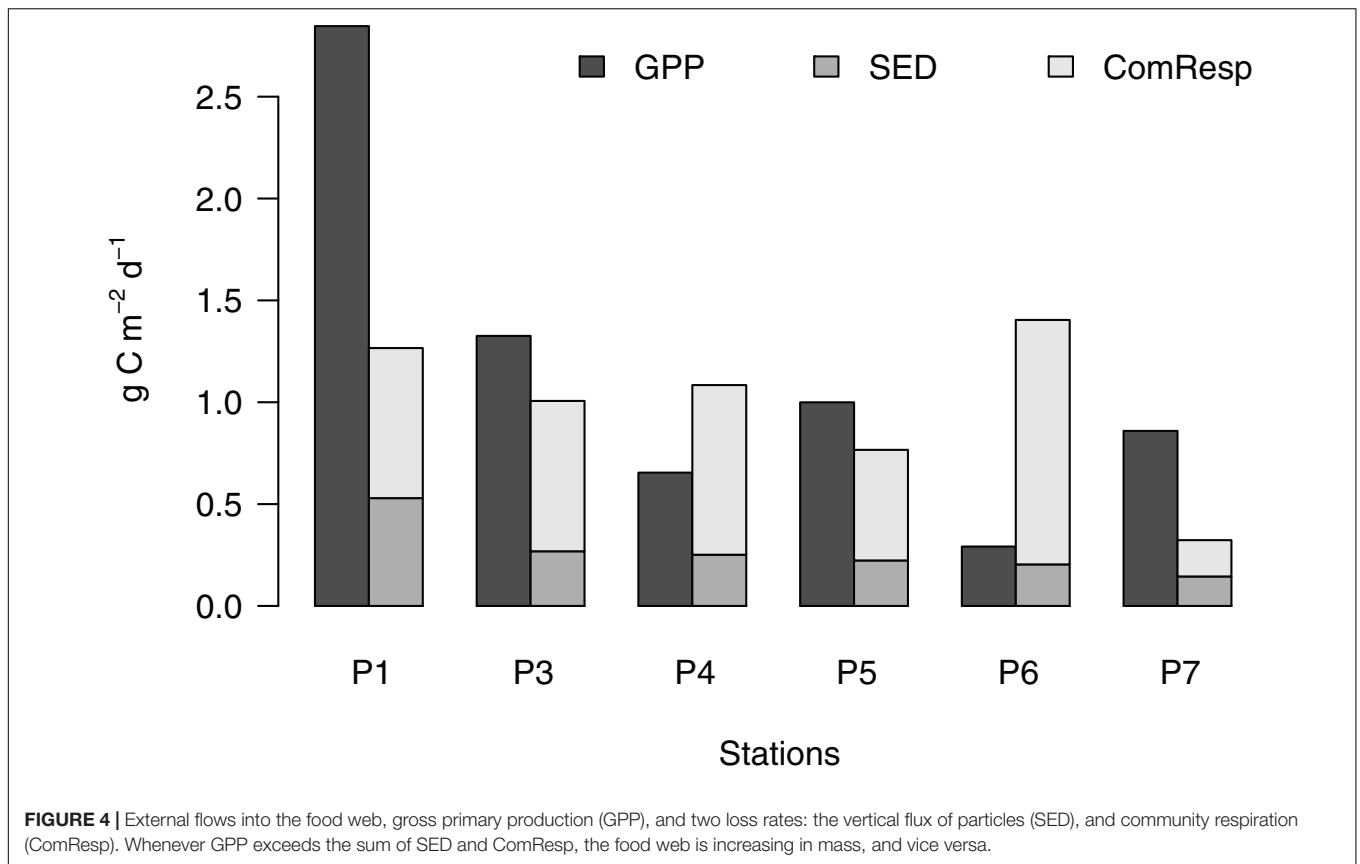
revealed no discernible pattern related to the successional stages, and varied between $80\text{--}380 \text{ mg C m}^{-2}$, and $360\text{--}840 \text{ mg C m}^{-2}$, for the small and large fractions, respectively.

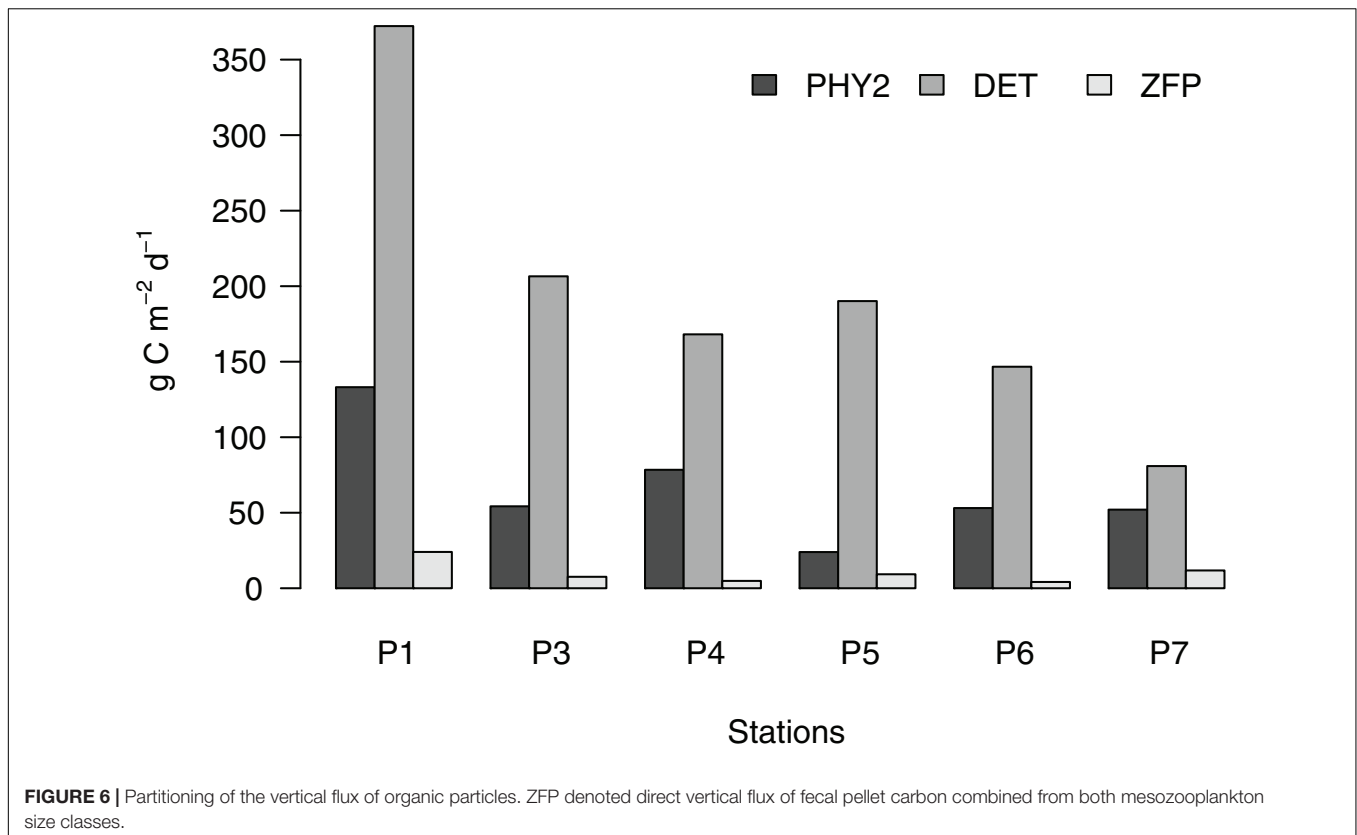
External Flows

The measured external flows were the gross primary production (GPP) into the system, and two competing flows out of the system, respiration and sedimentation. GPP decreased from 2.85 to 1.33 to $0.65 \text{ g C m}^{-2} \text{d}^{-1}$ and varied between 0.29 and $1 \text{ g C m}^{-2} \text{d}^{-1}$, during the post bloom phases (Figure 4).

Respiration always exceeded the sedimentation losses (Figure 4), indicating the relative efficiency of the food web in retaining energy resources. The inverse reconstruction partitioned the majority of the community respiration during the pre-bloom phase to bacteria ($500 \text{ mg C m}^{-2} \text{d}^{-1}$, corresponding to 68% of the community respiration), but the rate and proportion decreased rapidly as the bloom progressed (to 50 and 33% at peak and late bloom stages, respectively). Concomitantly, the respiration of the phototrophic compartments increased from 9% during the pre-bloom state to >16% thereafter, and the sum of grazer respiration from 23 to >60% as the community matured during late and post bloom stages (Figure 5).

Sedimentation was relatively higher ($251\text{--}529 \text{ mg C m}^{-2} \text{d}^{-1}$) during the bloom stage in May, and $145\text{--}223 \text{ mg C m}^{-2} \text{d}^{-1}$ in August. The vertical flux of organic particles increased from 19 to 20 to 38% of the GPP during the early, peak, and late bloom phases in May, and varied between low values of 17% (P5) to as high as 70% (P7) during post bloom phases. Overall, sedimentation losses were 5.8% of the total particulate carbon standing stock during the early bloom stage,





and only <3% thereafter. The vertical flux of organic particles was predominantly partitioned between detritus (56–85%) and phytoplankton (11–36%), while zooplankton fecal pellets contributed a minor fraction (**Figure 6**).

The difference between the carbon flows in and out of the system shows the growth or shrinkage of the food web. **Figure 4** shows the sum of the external flows, indicating a rapid growth of the system mass during the early bloom phase, where GPP exceeded the sum of respiration and sedimentation losses by $1.6 \text{ g C m}^{-2} \text{ d}^{-1}$. This increase of the food web continued during the peak bloom phase at a slower pace ($0.3 \text{ g C m}^{-2} \text{ d}^{-1}$) and turned into system shrinkage at the late stage of the bloom ($-0.4 \text{ g C m}^{-2} \text{ d}^{-1}$). The post bloom stages showed variation in both directions (**Figure 4**). The food web turned net heterotrophic during the bloom decline phase, and in station P6 during the post bloom stage, where GPP was 78 and 24% of community respiration, respectively.

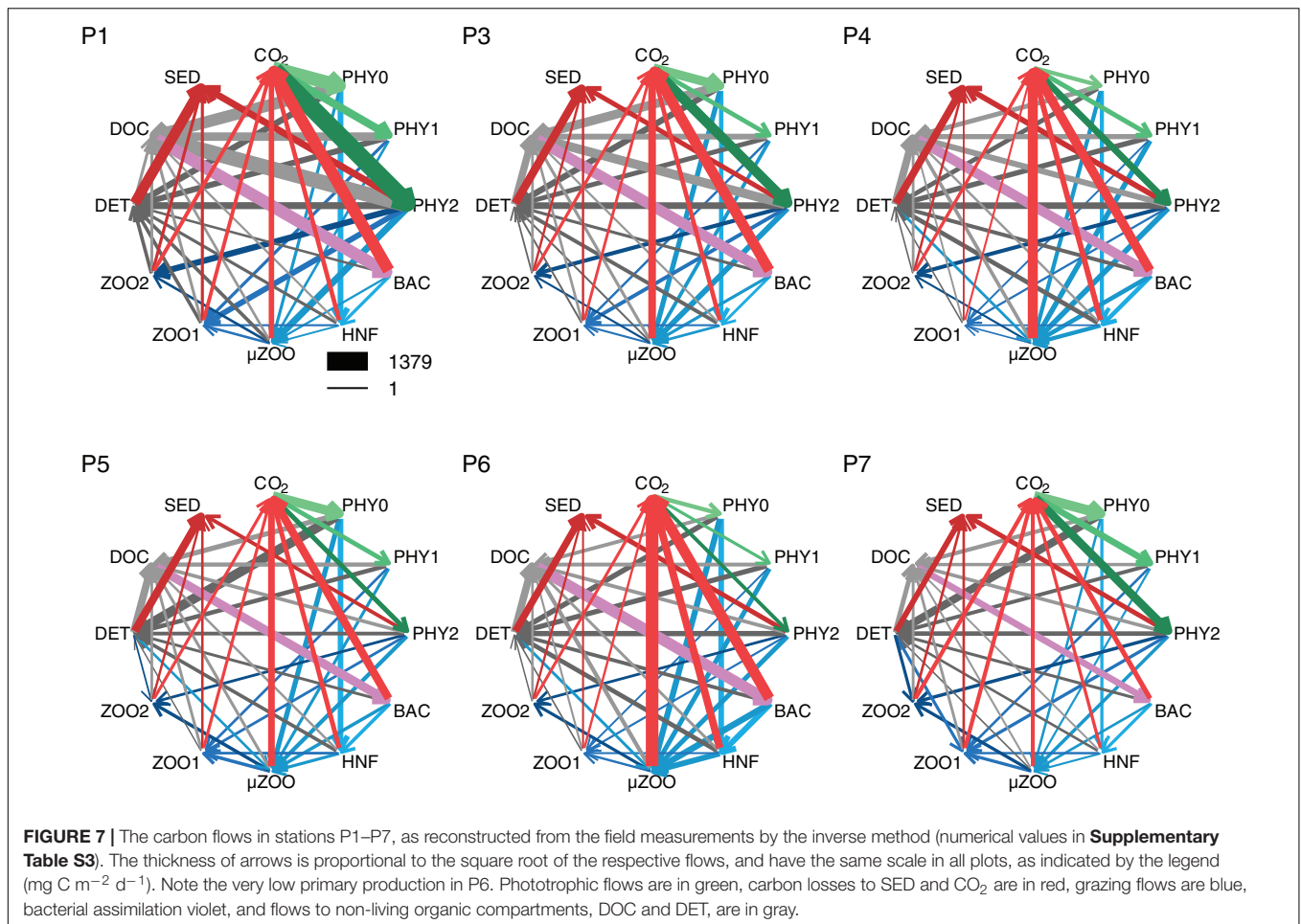
Reconstructed Internal Food Web Flows

The internal flow pattern was dominated by two flows, exudation by phytoplankton into the DOC pool, and bacterial assimilation of DOC (**Figure 7** and **Supplementary Table S3**). Phytoplankton exudation varied by more than an order of magnitude and was highest during the early bloom stage ($1565 \text{ mg C m}^{-2} \text{ d}^{-1}$), dropped rapidly thereafter to $620 \text{ mg C m}^{-2} \text{ d}^{-1}$ during the peak bloom, and to $205 \text{ mg C m}^{-2} \text{ d}^{-1}$ and below in late and post bloom stages. Phytoplankton exudation formed a decreasing proportion, from 55 to 49 to 31%, of the GPP during the bloom

stages in May. During the post bloom stages in August the dissolved fraction of GPP was generally low, 9–12% (P5 and P7), and 26%, in P6. The other significant source of DOC was dissolution from detritus (up to $170 \text{ mg C m}^{-2} \text{ d}^{-1}$), which formed 1.6 to 4.6% of the detritus biomass, and 20 to 56% of the total food web DOC release (apart from the negligible <1% during the early bloom stage). Heterotrophic grazers contributed little to the DOC pool ($20\text{--}51 \text{ mg C m}^{-2} \text{ d}^{-1}$), which formed 2–18% of the total food web DOC release.

Bacterial assimilation was highest during the early and peak bloom stages, 535 and $406 \text{ mg C m}^{-2} \text{ d}^{-1}$, respectively, and decreased thereafter to $329 \text{ mg C m}^{-2} \text{ d}^{-1}$ and below (except $439 \text{ mg C m}^{-2} \text{ d}^{-1}$ in station P6). Bacterial assimilation was in correspondence with the rate of fresh DOC production, but statistically not significantly (Pearson $r = 0.77$, $p = 0.07$, $n = 6$).

Other internal flows were related to grazing by the zooplankton compartments (collectively $240\text{--}664 \text{ mg C m}^{-2} \text{ d}^{-1}$), as well as zooplankton mortality and defecation (up to $52 \text{ mg C m}^{-2} \text{ d}^{-1}$). Detritus formation was relatively stable ($401\text{--}468 \text{ mg C m}^{-2} \text{ d}^{-1}$) during the bloom phases in May, and somewhat more variable in August ($331\text{--}498 \text{ mg C m}^{-2} \text{ d}^{-1}$). The percentage of GPP channeled to detritus increased from 16 to 31% to 61% during the bloom progression in May and varied from 38% (P7) to 147% (P6) in August. The sources and sinks of detritus were approximately balanced, when averaged over all stations. The ratio between the sum of sources and sinks of detritus varied between 1.25 and 0.78 (mean 1.01 ± 0.19). On average half of the detritus ($194 \pm 98 \text{ mg C m}^{-2} \text{ d}^{-1}$) settled out



of the water column, the other half was almost equally partitioned between dissolution ($119 \pm 70 \text{ mg C m}^{-2} \text{ d}^{-1}$) and grazing ($119 \pm 81 \text{ mg C m}^{-2} \text{ d}^{-1}$). On average, microzooplankton was the main detritivorous group ($86 \text{ mg C m}^{-2} \text{ d}^{-1}$; 62% of detritivory), followed by large ($18 \text{ mg C m}^{-2} \text{ d}^{-1}$; 21%) and small ($14 \text{ mg C m}^{-2} \text{ d}^{-1}$; 17%) mesozooplankton.

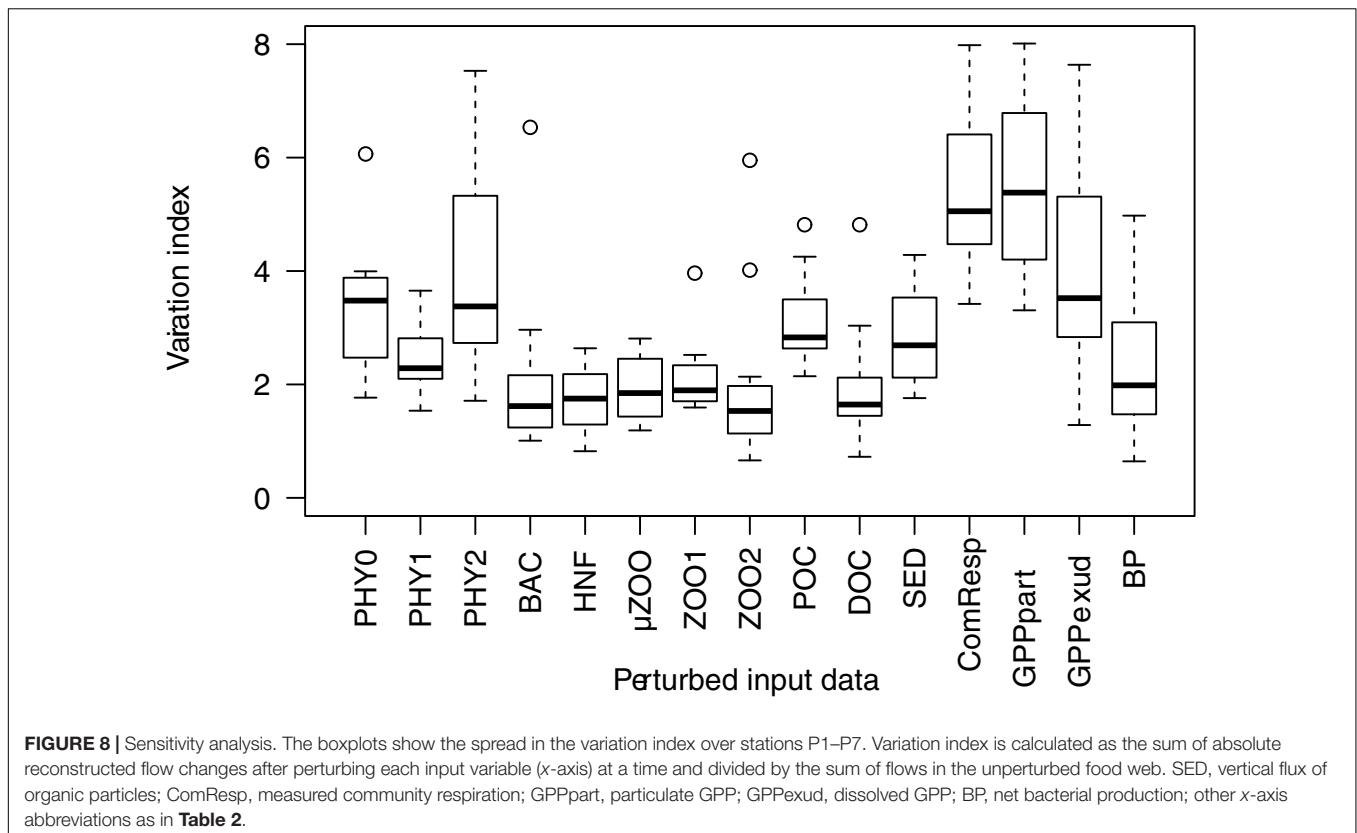
Sensitivity Analysis

To increase confidence in the model, we analyzed the robustness of the reconstructed fluxes to changes in the 10 measured compartment biomasses and the five measured flows. The sensitivity analysis was done by perturbing each measured input at a time by $\pm 10\%$, while keeping other variables unchanged. The six stations and fifteen input variables, each increased and decreased by 10%, resulted in 180 perturbed food web models and 178 successful solutions. Most flow values changed somewhat after perturbation. For each solution we calculated the absolute sum of these changes. The sum of absolute flow changes, as percentage of the sum of flows in the original unperturbed system was calculated as a variation index for each of the input variable. We used both, the minimum norm, and the likelihood approaches to test the model sensitivity. Both methods gave similar results and for consistency we here present the likelihood approach.

Sensitivity analysis shows that the variation index always remained below 10%, regardless of the input variable perturbed (**Figure 8**). Nevertheless, the overall sensitivity of the reconstructions depended on which input variable was perturbed. Firstly, the inverse solutions tended to be less sensitive to perturbations in the standing stock biomass estimates (PHY0, PHY1, ..., DOC), and more sensitive to boundary condition rate measurements (SED, ComResp, and GPP). The high variability within the individual effects (1–7%; **Figure 8**) indicated that the food web sensitivity during different stages of the bloom development also varied considerably. In summary, our sensitivity analysis indicates that small systematic errors in the input data would not affect the inverse solution in a disproportionate manner.

DISCUSSION

The seasonal stages and community maturation were reflected in the considerable diversity of the food web flows, even though the structural assumptions of the food webs were kept constant. The over-arching commonality was the dissolved fraction as the largest organic carbon pool. Only during the peak and decline phases of the algal bloom did the substantial



build-up of phytoplankton and detritus, respectively, result in relatively lower difference between the dissolved and particulate organic carbon pools.

The input and consumption of DOC revealed considerable seasonal variation. The food web DOC release decreased rapidly during the bloom in May (from 1572 to 275 mg C m⁻² d⁻¹) and remained modest during post-bloom stages (<200 mg C m⁻² d⁻¹). Presumably the large input in spring was due to the predominance of colonial *Phaeocysts* during the bloom phase, which is known to produce conspicuous amounts of extracellular polysaccharides (Billen and Fontigny, 1987; Verity et al., 2007; Thornton, 2014). The released DOC was readily assimilated by bacteria (122–534 mg C m⁻² d⁻¹), but at a high respiration cost (200–504 mg C m⁻² d⁻¹; but in P7 only 58 mg C m⁻² d⁻¹). This led to a substantial seasonal dynamics of bacterial growth efficiency, from low values of 6% during the early and peak bloom phases to 16% at the bloom decline phase. The bacterial growth efficiency was variable, 22, 13, and 53%, during the post bloom stages. These values are within the range of literature reports from various oceanic systems (del Giorgio and Cole, 1998, and references therein). Our evidence thus points that the blooms of colonial *Phaeocysts* are a fresh source of DOC, but the quality of this substrate, low in nitrogen compounds, is low for bacterial consumption (Billen and Fontigny, 1987; Carlson et al., 1999; Williams et al., 2016), and the assimilation by the ambient assemblages has a high energetic cost. Further, bacteria consumed only 33–50% of the freshly released DOC during the early and peak

bloom phases, but as much as 81% during the decline bloom phase. During the post-bloom stages in August the bacterial carbon assimilation matched fairly closely the instantaneous DOC release (80–86% in P5 and P7) or even exceeded it (152% in P6).

The seasonality, driven by the phytoplankton production and DOC release, cascaded through the food web, being more clearly expressed at the lower part of the food web. The seasonality in fresh DOC release was clearly discernible in bacterial biomass accumulation, which almost doubled from 437 mg C m⁻² at pre-bloom stage to 803 and 866 mg C m⁻² at peak and late bloom stages, a hallmark of *Phaeocysts* bloom associated bacterial activity (Billen and Fontigny, 1987). There was thus a time lag between the high DOC release at the early bloom stage, and the bacterial production and biomass response, further supporting only modest degradability of the *Phaeocysts* exudates (Carlson et al., 1999; Williams et al., 2016). Also, heterotrophic nanoflagellates revealed a very rapid biomass build up from 100 to 613 mg C m⁻² during the course of the bloom, suggesting a swift response to the increased resource availability. In contrast, microzooplankton, composed of large protists in our model, revealed only broad seasonal shifts in biomass between May and August, uncoupled from the dynamics of the bloom. The trophic cascade signal become indiscernible in the response of mesozooplankton compartments.

Another conspicuous seasonal feature was a shift from a system, where the POC pool was dominated by phytoplankton during the early bloom stage, to a system dominated by detritus.

This indicates that during the polar winter the water column comes to be low in organic particles, and the new seasonal build-up of POC is initiated by phytoplankton. The rapid build-up of detritus during the early, peak, and decline phases of the bloom, from 220 to 4425 to 6667 mg C m^{-2} were in line with a substantial mortality loss of phytoplankton (240–347 $\text{mg C m}^{-2} \text{d}^{-1}$) already at an early seasonal stage of the community maturation.

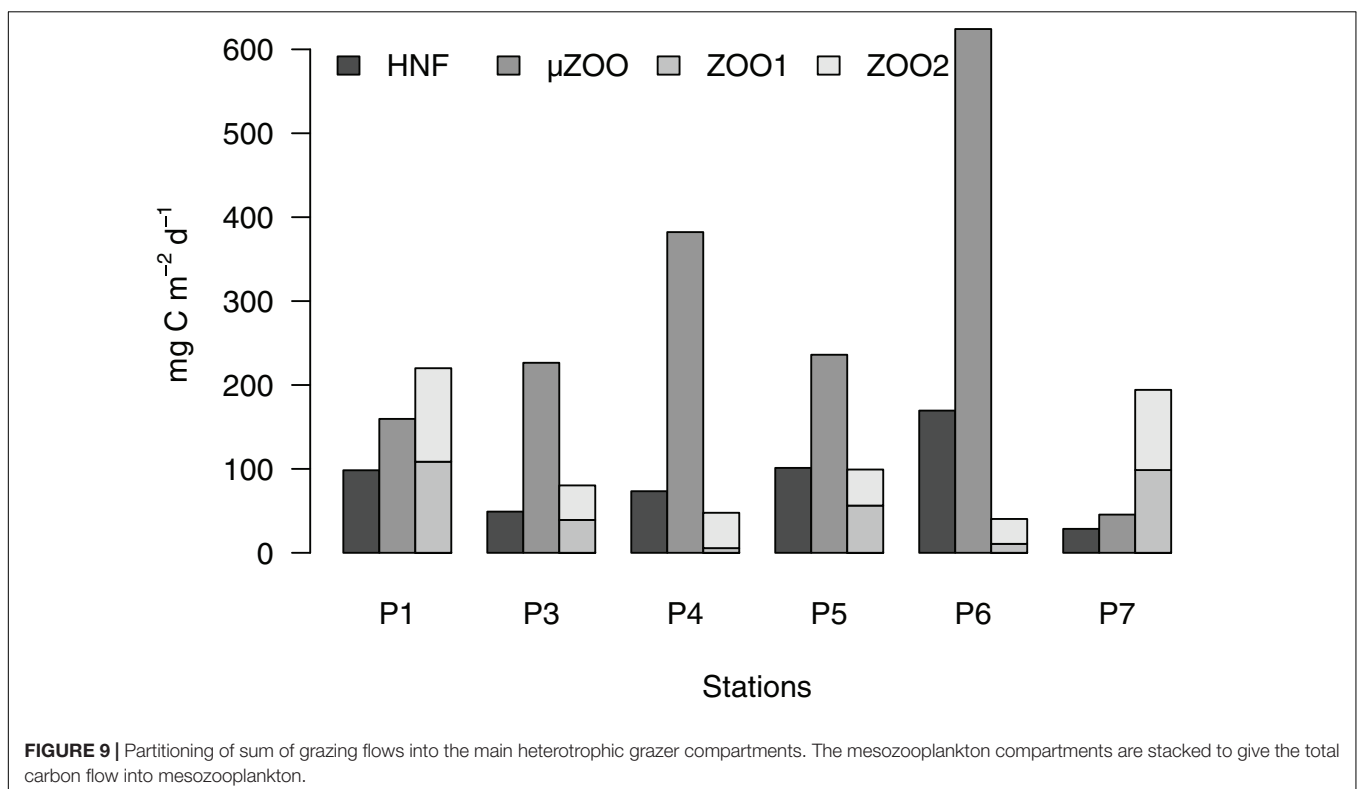
The conspicuous shift in organic particle composition from phytoplankton to detritus dominance had a profound effect on zooplankton feeding. Mesozooplankton herbivory decreased from 92 to 78% to 69% of food intake during the bloom progression and was only between 20 and 28% during post bloom stages. During the post bloom stages the drop in herbivory was compensated by detritivory (27–62% of food intake), and carnivory (consumption of HNF and microzooplankton; 17–45% of food intake). The pattern was paralleled by microzooplankton, with rapid drop of herbivory from 97 to 72% to 45% during the bloom progression and staying at that level (32–55%) during the post bloom stages in August. The microzooplankton diet changed predominantly to detritus (27–43% of food intake), with carnivory (4–15%) and bacterivory (7–18%) of lower importance in August. The available evidence thus supports a flexible omnivorous feeding behavior of the dominant zooplankton groups, which is in line with recent studies from the Arctic (Forest et al., 2011; Vernet et al., 2017).

Community respiration was 26, 55, and 126% of GPP in the early, peak, and late bloom stages, indicating switching from net-phototrophy to net-heterotrophy as the spring bloom matured. During the post-bloom stages, the ratio of community respiration

to GPP varied even more, from 21% (P7) to 410% (P6), suggesting high spatial heterogeneity in the physical water mass as well as food webs properties over relatively short distances.

Due to the logistical reasons, compartment biomasses were measured only once per station, and rates of mass change were only approximated by the inverse analysis (Figure 3). Summing up the changes in particulate pools, i.e., the living compartments and detritus, gave the rate of mass change of the particulate organic carbon pool. As expected, there was a strong particulate biomass build-up during the early bloom phase (509 $\text{mg C m}^{-2} \text{d}^{-1}$), which turned into a biomass decrease already during the peak (−80 $\text{mg C m}^{-2} \text{d}^{-1}$), and even more so during the bloom decline phase (−509 $\text{mg C m}^{-2} \text{d}^{-1}$). During the post-bloom stages, the biomass change rates varied even more, from 516 $\text{mg C m}^{-2} \text{d}^{-1}$ (P7) to −962 $\text{mg C m}^{-2} \text{d}^{-1}$ (P6), underlining the high heterogeneity of water masses in close spatial proximity in the Arctic marginal ice zone. The rate of biomass change divided by the GPP indicates the efficiency of the food web to convert primary production to particulate matter. The ratio was relatively low, 0.18, during the early bloom phase, and the positive values during post bloom stages ranged from 0.17 (P5) to 0.6 (P7).

The sum of grazing flows by heterotrophic nanoflagellates, micro- and mesozooplankton ranged from 268 to 834 $\text{mg C m}^{-2} \text{d}^{-1}$, with no clear seasonal pattern. The total grazing pressure increased from 17 to 27 to 77% of GPP, as the bloom progressed in May. In August the grazing pressure was 31–44%, except in P6, where it was exceptionally high (286%). This suggests that the high gross primary production



during a *Phaeocystis* dominated bloom does not support a high carbon turnover in the grazing food web. This is in line with the poor usability of *Phaeocystis* derived dissolved organic carbon by heterotrophic bacteria.

Partitioning the carbon turnover by heterotrophic grazers revealed high variability, an increasing role of microzooplankton during the bloom progression in May, and approximately equal mean apportionment between the two size classes of mesozooplankton (Figure 9). Averaging the carbon intake over all the six stations revealed microzooplankton as the most important grazer group ($279 \pm 202 \text{ mg C m}^{-2} \text{ d}^{-1}$), followed by the sum of the two mesozooplankton compartments ($113 \pm 76 \text{ mg C m}^{-2} \text{ d}^{-1}$), and heterotrophic nanoflagellates ($87 \pm 49 \text{ mg C m}^{-2} \text{ d}^{-1}$). Microzooplankton has been recognized as a main grazer compartment globally, estimated to consume over half of the daily global planktonic primary production (Calbet and Landry, 2004; Schmoker et al., 2013). Further, several specialized microzooplankton taxa, like the heterotrophic *Gymnodinium* and *Gyrodinium* species, and tintinnid ciliates, are known to prey upon *Phaeocystis* cells (Grattepanche et al., 2011; Swalethorp et al., 2019). This takes place particularly in the late bloom stage, when single cells are often released from colonies possibly when nutrients become limited (Jakobsen and Tang, 2002; Nejstgaard et al., 2007).

AUTHOR CONTRIBUTIONS

KO participated in the cruises, designed the study, conducted the model analysis, and was in charge of the writing. EH, MV,

PL, GF, MS-M, MP, and MR provided data for the model, participated in food web construction, data interpretation and writing. EH provided all the mesozooplankton data and searched or measured the values for mesozooplankton carbon content. MV provided data on particulate and dissolved primary production. PL and GF contributed with the microzooplankton data. MS-M provided the data for community respiration. MP provided data for microbial components and TOC. MR organized the cruise, was in charge of the project, and provided the data for chlorophyll, POC, and vertical flux.

FUNDING

This work was funded by the Estonian Research Council (Grant 1574P), and the Norwegian Research Council through the project CarbonBridge (Project Number 226415).

ACKNOWLEDGMENTS

We thank the captain and crew of the R/V Helmer Hanssen for their helpful cooperation.

SUPPLEMENTARY MATERIAL

The Supplementary Material for this article can be found online at: <https://www.frontiersin.org/articles/10.3389/fmars.2019.00244/full#supplementary-material>

REFERENCES

- Arrigo, K. R., and van Dijken, G. L. (2015). Continued increases in Arctic Ocean primary production. *Prog. Oceanogr.* 136, 60–70. doi: 10.1016/j.pocean.2015.05.002
- Basedow, S. L., Sundfjord, A., von Appen, W.-J., Halvorsen, E., Kwasniewski, S., and Reigstad, M. (2018). Seasonal variation in transport of zooplankton into the arctic basin through the atlantic gateway. *Fram. Strait. Front. Mar. Sci.* 5:194. doi: 10.3389/fmars.2018.00194
- Beszczynska-Moller, A., Fahrbach, E., Schauer, U., and Hansen, E. (2012). Variability in Atlantic water temperature and transport at the entrance to the Arctic Ocean, 1997–2010. *ICES J. Mar. Sci.* 69, 852–863. doi: 10.1093/icesjms/fss056
- Billen, G., and Fontigny, A. (1987). Dynamics of a phaeocystis-dominated spring bloom in Belgian coastal waters. II. Bacterioplankton dynamics. *Mar. Ecol. Prog. Ser.* 37, 249–257. doi: 10.3354/meps037249
- Blais, M., Ardyna, M., Gosselin, M., Dumont, D., Bélanger, S., Tremblay, J. É., et al. (2017). Contrasting interannual changes in phytoplankton productivity and community structure in the coastal canadian arctic ocean: variability in arctic phytoplankton dynamics. *Limnol. Oceanogr.* 62, 2480–2497. doi: 10.1002/lno.10581
- Børsheim, K., and Bratbak, G. (1987). Cell volume to cell carbon conversion factors for a bacterivorous *Monas* sp. enriched from seawater. *Mar. Ecol. Prog. Ser.* 36, 171–175. doi: 10.3354/meps036171
- Calbet, A., and Landry, M. R. (2004). Phytoplankton growth, microzooplankton grazing, and carbon cycling in marine systems. *Limnol. Oceanogr.* 49, 51–57. doi: 10.4319/lo.2004.49.1.0051
- Carlson, C., Bates, N., Ducklow, H., and Hansell, D. (1999). Estimation of bacterial respiration and growth efficiency in the Ross Sea, Antarctica. *Aquat. Microb. Ecol.* 19, 229–244. doi: 10.3354/ame019229
- Chan, F. T., Stanislawczyk, K., Sneekes, A. C., Dvoretzky, A., Gollasch, S., Minchin, D., et al. (2018). Climate change opens new frontiers for marine species in the Arctic: current trends and future invasion risks. *Glob. Chang. Biol.* 25, 25–38. doi: 10.1111/gcb.14469
- Chénard, C., and Lauro, F. M. (2017). “Exploring the viral ecology of high latitude aquatic systems,” in *Microbial Ecology of Extreme Environments*, eds C. Chénard and F. M. Lauro (Cham: Springer International Publishing), 185–200. doi: 10.1007/978-3-319-51686-8_8
- De Laender, F., Soetaert, K., and Middelburg, J. J. (2010). Inferring chemical effects on carbon flows in aquatic food webs: methodology and case study. *Environ. Pollut.* 158, 1775–1782. doi: 10.1016/j.envpol.2009.11.009
- del Giorgio, P. A., and Cole, J. J. (1998). Bacterial growth efficiency in natural aquatic systems. *Annu. Rev. Ecol. Syst.* 29, 503–541. doi: 10.1146/annurev.ecolsys.29.1.503
- Ducklow, H. (2000). “Bacterial production and biomass in the oceans,” in *Microbial Ecology of the Oceans*, ed. D. Kirchman (New York, NY: Wiley), 85–120.
- Falkowski, P. G., Dubinsky, Z., and Wyman, K. (1985). Growth-irradiance relationships in phytoplankton: growth-irradiance relationships. *Limnol. Oceanogr.* 30, 311–321. doi: 10.4319/lo.1985.30.2.0311
- Fischer, G., and Wefer, G. (2013). “Sampling, preparation and analysis of marine particulate matter,” in *Geophysical Monograph Series*, eds D. C. Hurd and D. W. Spencer (Washington, DC: American Geophysical Union), 391–397. doi: 10.1029/GM063p0391
- Forest, A., Tremblay, J. É., Gratton, Y., Martin, J., Gagnon, J., Darnis, G., et al. (2011). Biogenic carbon flows through the planktonic food web of the Amundsen Gulf (Arctic Ocean): a synthesis of field measurements and inverse modeling analyses. *Prog. Oceanogr.* 91, 410–436. doi: 10.1016/j.pocean.2011.05.002
- Gast, R. J., Moran, D. M., Dennett, M. R., and Caron, D. A. (2007). Kleptoplasty in an Antarctic dinoflagellate: caught in evolutionary transition? *Environ. Microbiol.* 9, 39–45. doi: 10.1111/j.1462-2920.2006.01109.x

- González-Eguino, M., Neumann, M. B., Arto, I., Capellán-Perez, I., and Faria, S. H. (2017). Mitigation implications of an ice-free summer in the Arctic Ocean. *Earths Future* 5, 59–66. doi: 10.1002/2016EF000429
- Grattepanche, J.-D., Vincent, D., Breton, E., and Christaki, U. (2011). Microzooplankton herbivory during the diatom-Phaeocystis spring succession in the eastern English Channel. *J. Exp. Mar. Biol. Ecol.* 404, 87–97. doi: 10.1016/j.jembe.2011.04.004
- Graversen, R. G., Mauritsen, T., Tjernström, M., Källén, E., and Svensson, G. (2008). Vertical structure of recent Arctic warming. *Nature* 451, 53–56. doi: 10.1038/nature06502
- Gregg, W. W., Conkright, M. E., Ginoux, P., O'Reilly, J. E., and Casey, N. W. (2003). Ocean primary production and climate: global decadal changes. *Geophys. Res. Lett.* 30:1809. doi: 10.1029/2003GL016889
- Hansen, H. (1997). Das Mesozooplankton im Laptevmeer und östlichen Nansen-Becken – Verteilung und Gemeinschaftsstrukturen im Spätsommer (Mesozooplankton of the Laptev Sea and the adjacent eastern Nansen Basin – distribution and community structure in late summer). *Helgol. Mar. Res.* 229:131. doi: 10.2312/BzP_0229_1997
- Hill, V., Ardyna, M., Lee, S. H., and Varela, D. E. (2018). Decadal trends in phytoplankton production in the Pacific Arctic Region from 1950 to 2012. *Deep Sea Res. Part II Top. Stud. Oceanogr.* 152, 82–94. doi: 10.1016/j.dsr2.2016.12.015
- Hirche, H.-J., and Kosobokova, K. (2003). Early reproduction and development of dominant calanoid copepods in the sea ice zone of the Barents Sea – need for a change of paradigms? *Mar. Biol.* 143, 769–781. doi: 10.1007/s00227-003-1122-8
- Holm-Hansen, O., Lorenzen, C. J., Holmes, R. W., and Strickland, J. D. H. (1965). Fluorometric Determination of Chlorophyll. *ICES J. Mar. Sci.* 30, 3–15. doi: 10.1093/icesjms/30.1.3
- Hopcroft, R. R., Kosobokova, K. N., and Pinchuk, A. I. (2010). Zooplankton community patterns in the Chukchi Sea during summer 2004. *Deep Sea Res. Part II Top. Stud. Oceanogr.* 57, 27–39. doi: 10.1016/j.dsr2.2009.08.003
- Jakobsen, H., and Tang, K. (2002). Effects of protozoan grazing on colony formation in *Phaeocystis globosa* (Prymnesiophyceae) and the potential costs and benefits. *Aquat. Microb. Ecol.* 27, 261–273. doi: 10.3354/ame027261
- Jeong, H., Yoo, Y., Kim, S., and Kang, N. (2004). Feeding by the heterotrophic dinoflagellate *Protoperidinium bipes* on the diatom *Skeletonema costatum*. *Aquat. Microb. Ecol.* 36, 171–179. doi: 10.3354/ame036171
- Kahru, M., Lee, Z., Mitchell, B. G., and Nevison, C. D. (2016). Effects of sea ice cover on satellite-detected primary production in the Arctic Ocean. *Biol. Lett.* 12, 20160223. doi: 10.1098/rsbl.2016.0223
- Kashiwase, H., Ohshima, K. I., Nihashi, S., and Eicken, H. (2017). Evidence for ice-ocean albedo feedback in the Arctic Ocean shifting to a seasonal ice zone. *Sci. Rep.* 7:8170. doi: 10.1038/s41598-017-08467-z
- Kirchman, D. (2001). Measuring bacterial biomass production and growth rates from leucine incorporation in natural aquatic environments. *Methods Microbiol.* 30, 227–237. doi: 10.1016/S0580-9517(01)30047-8
- Kones, J. K., Soetaert, K., van Oevelen, D., Owino, J. O., and Mavuti, K. (2006). Gaining insight into food webs reconstructed by the inverse method. *J. Mar. Syst.* 60, 153–166. doi: 10.1016/j.jmarsys.2005.12.002
- Kwasniewski, S. (2003). Distribution of *Calanus* species in Kongsfjorden, a glacial fjord in Svalbard. *J. Plankton Res.* 25, 1–20. doi: 10.1093/plankt/25.1.1
- Lovejoy, C., Massana, R., and Pedros-Alío, C. (2006). Diversity and Distribution of Marine Microbial Eukaryotes in the Arctic Ocean and Adjacent Seas. *Appl. Environ. Microbiol.* 72, 3085–3095. doi: 10.1128/AEM.72.5.3085-3095.2006
- Luong, A. D., De Laender, F., Olsen, Y., Vadstein, O., Dewulf, J., and Janssen, C. R. (2014). Inferring time-variable effects of nutrient enrichment on marine ecosystems using inverse modelling and ecological network analysis. *Sci. Total Environ.* 493, 708–718. doi: 10.1016/j.scitotenv.2014.06.027
- Maraóón, E., Cermeó, P., Rodríguez, J., Zubkov, M. V., and Harris, R. P. (2007). Scaling of phytoplankton photosynthesis and cell size in the ocean. *Limnol. Oceanogr.* 52, 2190–2198. doi: 10.4319/lo.2007.52.5.2190
- Meersche, K. V., den Soetaert, K., and Oevelen, D. V. (2009). xsample(): an r function for sampling linear inverse problems. *J. Stat. Softw.* 30, c01. doi: 10.18637/jss.v030.c01
- Menden-Deuer, S., and Lessard, E. J. (2000). Carbon to volume relationships for dinoflagellates, diatoms, and other protist plankton. *Limnol. Oceanogr.* 45, 569–579. doi: 10.4319/lo.2000.45.3.0569
- Møller, E. F. (2004). Sloppy feeding in marine copepods: prey-size-dependent production of dissolved organic carbon. *J. Plankton Res.* 27, 27–35. doi: 10.1093/plankt/fbh147
- Møller, E. F., Thor, P., and Nielsen, T. G. (2003). Production of DOC by *Calanus finmarchicus*, *C. glacialis* and *C. hyperboreus* through sloppy feeding and leakage from fecal pellets. *Mar. Ecol. Prog. Ser.* 262, 185–191. doi: 10.3354/meps262185
- Nejstgaard, J. C., Tang, K. W., Steinke, M., Dutz, J., Koski, M., Antajan, E., et al. (2007). “Zooplankton grazing on Phaeocystis: a quantitative review and future challenges,” in *Phaeocystis, Major Link in the Biogeochemical Cycling of Climate-Relevant Elements*, eds M. A. van Leeuwe, J. Stefels, S. Belviso, C. Lancelot, P. G. Verity, and W. W. C. Gieskes (Dordrecht: Springer), 147–172. doi: 10.1007/978-1-4020-6214-8_12
- Neukermans, G., Oziel, L., and Babin, M. (2018). Increased intrusion of warming Atlantic water leads to rapid expansion of temperate phytoplankton in the Arctic. *Glob. Chang. Biol.* 24, 2545–2553. doi: 10.1111/gcb.14075
- Nielsen, E. S. (1952). The use of radio-active carbon (C14) for measuring organic production in the sea. *ICES J. Mar. Sci.* 18, 117–140. doi: 10.1093/icesjms/18.2.117
- Nöthig, E.-M., Bracher, A., Engel, A., Metfies, K., Niehoff, B., Peeken, I., et al. (2015). Summertime plankton ecology in Fram Strait—a compilation of long- and short-term observations. *Polar Res.* 34:23349. doi: 10.3402/polar.v34.23349
- Olsen, Y., Agustí, S., Andersen, T., Duarte, C. M., Gasol, J. M., Gismervik, I., et al. (2006). A comparative study of responses in plankton food web structure and function in contrasting European coastal waters exposed to experimental nutrient addition. *Limnol. Oceanogr.* 51, 488–503. doi: 10.4319/lo.2006.51.1_part_2.0488
- Olseng, C., Naustvoll, L., and Paasche, E. (2002). Grazing by the heterotrophic dinoflagellate *protoperidinium steinii* on a ceratium bloom. *Mar. Ecol. Prog. Ser.* 225, 161–167. doi: 10.3354/meps225161
- Oudot, C., Gerard, R., Morin, P., and Gningue, I. (1988). Precise shipboard determination of dissolved oxygen (Winkler procedure) for productivity studies with a commercial system I. *Limnol. Oceanogr.* 33, 146–150. doi: 10.4319/lo.1988.33.1.0146
- Parsons, T. R., Takahashi, M., and Hargrave, B. (2014). *Biological Oceanographic Processes*. Kent: Elsevier Science.
- Pedros-Alío, C., Potvin, M., and Lovejoy, C. (2015). Diversity of planktonic microorganisms in the Arctic Ocean. *Prog. Oceanogr.* 139, 233–243. doi: 10.1016/j.pocean.2015.07.009
- Polovina, J. J., Howell, E. A., and Abecassis, M. (2008). Ocean's least productive waters are expanding. *Geophys. Res. Lett.* 35:L03618. doi: 10.1029/2007GL031745
- Postel, L., Fock, H., and Hagen, W. (2000). “Biomass and abundance,” in *ICES Zooplankton Methodology Manual*, eds R. Harris, P. Wiebe, J. Lenz, H. R. Skjoldal, and M. Huntley (New York, NY: Academic Press), 83–192. doi: 10.1016/B978-012327645-2/50005-0
- Randelhoff, A., Reigstad, M., Chierici, M., Sundfjord, A., Ivanov, V., Cape, M., et al. (2018). Seasonality of the physical and biogeochemical hydrography in the inflow to the Arctic Ocean through fram strait. *Front. Mar. Sci.* 5:224. doi: 10.3389/fmars.2018.00224
- Richter, C. (1994). Regional and seasonal variability in the vertical distribution of mesozooplankton in the Greenland Sea. *Helgol. Mar. Res.* 154:87. doi: 10.2312/BzP_0154_1994
- Rieman, B., Simonsen, P., and Stensgaard, L. (1989). The carbon and chlorophyll content of phytoplankton from various nutrient regimes. *J. Plankton Res.* 11, 1037–1045. doi: 10.1093/plankt/11.5.1037
- Saint-Béat, B., Maps, F., and Babin, M. (2018). Unraveling the intricate dynamics of planktonic Arctic marine food webs. A sensitivity analysis of a well-documented food web model. *Prog. Oceanogr.* 160, 167–185. doi: 10.1016/j.pocean.2018.01.003
- Samhuri, J. F., Levin, P. S., and Harvey, C. J. (2009). Quantitative evaluation of marine ecosystem indicator performance using food web models. *Ecosystems* 12, 1283–1298.
- Sanders, R. W., Caron, D. A., and Berninger, U.-G. (1992). Relationships between bacteria and heterotrophic nanoplankton in marine and fresh waters: an inter-ecosystem comparison. *Mar. Ecol. Prog. Ser.* 86, 1–14.
- Schmoker, C., Hernández-León, S., and Calbet, A. (2013). Microzooplankton grazing in the oceans: impacts, data variability, knowledge gaps and future directions. *J. Plankton Res.* 35, 691–706. doi: 10.1093/plankt/fbt023
- Simon, M., and Azam, F. (1989). Protein content and protein synthesis rates of planktonic marine bacteria. *Mar. Ecol. Prog. Ser.* 51, 201–213. doi: 10.3354/meps051201

- Soetaert, K., and van Oevelen, D. (2009). Modeling food web interactions in benthic deep-sea ecosystems: a practical guide. *Oceanography* 22, 128–143. doi: 10.5670/oceanog.2009.13
- Stocker, T. (ed.) (2014). *Climate Change 2013: the Physical Science Basis: Working Group I Contribution to the Fifth Assessment Report of the Intergovernmental Panel on Climate Change*. New York, NY: Cambridge University Press.
- Stoecker, D., Johnson, M., deVargas, C., and Not, F. (2009). Acquired phototrophy in aquatic protists. *Aquat. Microb. Ecol.* 57, 279–310. doi: 10.3354/ame01340
- Straile, D. (1997). Gross growth efficiencies of protozoan and metazoan zooplankton and their dependence on food concentration, predator-prey weight ratio, and taxonomic group. *Limnol. Oceanogr.* 42, 1375–1385. doi: 10.4319/lo.1997.42.6.1375
- Stroeve, J., and Notz, D. (2018). Changing state of Arctic sea ice across all seasons. *Environ. Res. Lett.* 13:103001. doi: 10.1088/1748-9326/aade56
- Swalethorp, R., Dinasquet, J., Logares, R., Bertilsson, S., Kjellerup, S., Krabberød, A. K., et al. (2019). Microzooplankton distribution in the amundsen sea polynya (Antarctica) during an extensive Phaeocystis antarctica bloom. *Prog. Oceanogr.* 170, 1–10. doi: 10.1016/j.pocean.2018.10.008
- Thornton, D. C. O. (2014). Dissolved organic matter (DOM) release by phytoplankton in the contemporary and future ocean. *Eur. J. Phycol.* 49, 20–46. doi: 10.1080/09670262.2013.875596
- Tremblay, J. É., Bélanger, S., Barber, D. G., Asplin, M., Martin, J., Darnis, G., et al. (2011). Climate forcing multiplies biological productivity in the coastal Arctic Ocean: upwelling and productivity in the arctic. *Geophys. Res. Lett.* 38:L18604. doi: 10.1029/2011GL048825
- Tremblay, J. -É., Robert, D., Varela, D. E., Lovejoy, C., Darnis, G., Nelson, R. J., et al. (2012). Current state and trends in Canadian Arctic marine ecosystems: I. Primary production. *Clim. Change* 115, 161–178. doi: 10.1007/s10584-012-0496-3
- van Oevelen, D., Van den Meersche, K., Meysman, F. J. R., Soetaert, K., Middelburg, J. J., and Vézina, A. F. (2010). Quantifying food web flows using linear inverse models. *Ecosystems* 13, 32–45. doi: 10.1007/s10021-009-9297-6
- Verity, P. G., Brussaard, C. P., Nejstgaard, J. C., van Leeuwe, M. A., Lancelot, C., and Medlin, L. K. (2007). Current understanding of Phaeocystis ecology and biogeochemistry, and perspectives for future research. *Biogeochemistry* 83, 311–330.
- Vernet, M., Richardson, T. L., Metfies, K., Nöthig, E.-M., and Peeken, I. (2017). Models of plankton community changes during a warm water anomaly in arctic waters show altered trophic pathways with minimal changes in carbon export. *Front. Mar. Sci.* 4:160. doi: 10.3389/fmars.2017.00160
- Vézina, A., and Platt, T. (1988). Food web dynamics in the ocean. I. Best-estimates of flow networks using inverse methods. *Mar. Ecol. Prog. Ser.* 42, 269–287. doi: 10.3354/meps042269
- Vézina, A., Savenkoff, C., Roy, S., Klein, B., Rivkin, R., Therriault, J.-C., et al. (2000). Export of biogenic carbon and structure and dynamics of the pelagic food web in the Gulf of St. Lawrence Part 2. Inverse analysis. *Deep Sea Res. Part II Top. Stud. Oceanogr.* 47, 609–635. doi: 10.1016/S0967-0645(99)00120-4
- Wexels Riser, C., Wassmann, P., Olli, K., Pasternak, A., and Arashkevich, E. (2002). Seasonal variation in production, retention and export of zooplankton faecal pellets in the marginal ice zone and central Barents Sea. *J. Mar. Syst.* 38, 175–188.
- Williams, C. M., Dupont, A. M., Loevenich, J., Post, A. F., Dinasquet, J., and Yager, P. L. (2016). Pelagic microbial heterotrophy in response to a highly productive bloom of Phaeocystis antarctica in the Amundsen Sea Polynya, Antarctica. *Elem. Sci. Anthr.* 4:000102. doi: 10.12952/journal.elementa.000102
- Zhou, M., Carlotti, F., and Zhu, Y. (2010). A size-spectrum zooplankton closure model for ecosystem modelling. *J. Plankton Res.* 32, 1147–1165. doi: 10.1093/plankt/fbq054
- Zubkov, M. V., Burkill, P. H., and Topping, J. N. (2007). Flow cytometric enumeration of DNA-stained oceanic planktonic protists. *J. Plankton Res.* 29, 79–86. doi: 10.1093/plankt/fbl059

Conflict of Interest Statement: The authors declare that the research was conducted in the absence of any commercial or financial relationships that could be construed as a potential conflict of interest.

Copyright © 2019 Olli, Halvorsen, Vernet, Lavrentyev, Franzè, Sanz-Martin, Paulsen and Reigstad. This is an open-access article distributed under the terms of the Creative Commons Attribution License (CC BY). The use, distribution or reproduction in other forums is permitted, provided the original author(s) and the copyright owner(s) are credited and that the original publication in this journal is cited, in accordance with accepted academic practice. No use, distribution or reproduction is permitted which does not comply with these terms.